Published in final edited form as:

J Magn Reson Open. 2023 December ; 16-17: . doi:10.1016/j.jmro.2023.100123.

Inductively coupled, transmit-receive coils for proton MRI and X-nucleus MRI/MRS in small animals

Atsushi M. Takahashi[a,*], **Jitendra Sharma**[a,c,f,g], **David O. Guarin**[b,c], **Julie Miller**[d], **Hiroaki Wakimoto**[e], **Daniel P. Cahill**[e], **Yi-Fen Yen**[c]

[a]Department of Brain and Cognitive Sciences, Massachusetts Institute of Technology, McGovern Institute for Brain Research, Cambridge, MA 02139, USA

[b]Polarize ApS, Frederiksberg 1808, Denmark

[c]Athinoula A. Martinos Center for Biomedical Imaging, Department of Radiology, Massachusetts General Hospital, Charlestown, MA 02129, USA

[d]Department of Neurology, Massachusetts General Hospital, Boston, MA 02114, USA

[e]Department of Neurosurgery, Massachusetts General Hospital, Boston, MA 02114, USA

[f]Stanley Center for Psychiatric Research, Broad Institute, MIT, Cambridge, MA 02139, USA

[g]Tan and Yang Center for Autism Research, McGovern Institute for Brain Research, MIT, Cambridge MA 02139, USA

Abstract

We report several inductively coupled RF coil designs that are very easy to construct, produce high signal-to-noise ratio (SNR) and high spatial resolution while accommodating life support, anesthesia and monitoring in small animals. Inductively coupled surface coils were designed for hyperpolarized ^{13}C MR spectroscopic imaging (MRSI) of mouse brain, with emphases on the simplicity of the circuit design, ease of use, whole-brain coverage, and high SNR. The simplest form was a resonant loop designed to crown the mouse head for a snug fit to achieve full coverage of the brain with high sensitivity when inductively coupled to a broadband pick-up coil. Here, we demonstrated the coil's performance in hyperpolarized ^{13}C MRSI of a normal mouse and a glioblastoma mouse model at 4.7 T. High SNR exceeding 70:1 was obtained in the brain with good spatial resolution (1.53 mm × 1.53 mm). Similar inductively coupled loop for other X-nuclei can be made very easily in a few minutes and achieve high performance, as demonstrated in ^{31}P spectroscopy. Similar design concept was expanded to splitable, inductively coupled volume coils for high-resolution proton MRI of marmoset at 3T and 9.4T, to easily accommodate head restraint, vital-sign monitoring, and anesthesia delivery.

*Corresponding author.: atsushi1@mit.edu (A.M. Takahashi).

Declaration of Competing Interest

The authors declare that they have no known competing financial interests or personal relationships that could have appeared to influence the work reported in this paper.

Keywords

Inductively coupled RF coils; Hyperpolarized MRI; ^{31} P spectroscopy; Glioblastoma model; Marmoset

1. Introduction

Image resolution in MRI is limited by the signal-to-noise ratio (SNR) of the imaging system. Hyperpolarized ^{13} C (HP13C) MR spectroscopic imaging (MRSI) is a promising technique to image enzyme-catalyzed metabolic transformations *in vivo* with >10,000 enhancement [1]. However, obtaining good spatial resolution in mouse brain, for example, is still a challenge due to its small size and non-replenishable HP13C signals. Lifetime of hyperpolarization is characterized by the T_1 relaxation time of the ^{13} C labels. Majority of the HP13C substrates or contrast agents have a T_1 of less than 75 seconds in solution and even shorter (~less than 40 seconds) *in vivo*. Since the hyperpolarized signal is not recoverable, signal averaging over a long period of time is not a viable strategy to gain signal to noise (SNR) ratio, unlike the conventional MR spectroscopy (MRS). One clever way to improve SNR for HP13C-MRSI is to optimize the efficiency of pulse sequence designs and acquisition strategies. Much progress has been made in this research area to improve spatial resolution of HP13C imaging in mouse brain [2–8]. To the best of our knowledge, spatial resolution as high as 1 mm × 1 mm × 3.5 mm (or 3.5 uL voxel size) was achieved with a single-time-point chemical shift imaging (CSI) at 9.4T [3,4]. Of course, sequence strategies that helped to significantly improve spatial resolution in rats and other organs [9–12] can be applied to improve that in mouse brain imaging as well. Having higher degree of polarization will also help to improve SNR and hence, the spatial resolution, but this is outside the scope of this work. Another way to improve SNR is to increase the RF coil sensitivity. The goal of this work, which was motivated by the need for a better spatial resolution in HP13C imaging of mouse brain, is to investigate inductively coupled, transmit-receive coil designs to improve SNR (and hence, the spatial resolution) while keeping things practical - having the coil as close to the mouse brain as possible, for example, without the need to surgically implant the coil.

In addition to the consideration of coil proximity to the organ of interest, there are many constraints in the setup for animal imaging, in general, often including a nose cone and the tubing to deliver anesthetics, suction to remove excessive anesthetics, vital sign sensors, ear bars, etc. Having a coil design that simplifies the setup and yet matches closely to the anatomy of interest can improve workflow and increase SNR. Furthermore, conventional coil designs for X-nucleus (i.e., non-proton nucleus) require separate coils each tuned to a specific X-nucleus resonance frequency and can be time-consuming to build and expensive. A single coil design that can be used for ^{1} H or any X-nucleus MR acquisition with only a minor and inexpensive adjustment will be time-saving and economical.

Coupling of a resonant structure to the NMR/MRI system can be achieved by matching its impedance to that of the receiver system. Capacitive coupling is commonly used but inductive coupling is equally useful and has some intrinsic benefits like balancing the circuit

electrically to minimize electric field interaction with the sample or tissue. Derby et al. [13] demonstrate inductive coupling in the ^{31}P channel of a dual-tuned ^{31}P and ^{1}H birdcage coil for spectroscopic imaging in the human head. This coil design was the foundation for the first dual-tuned ^{13}C and ^{1}H birdcage coil by GE Healthcare for HP13C imaging in rodents [14,15].

The use of inductively coupled coils has also been explored in the realm of implanted coils. MRI RF coils are placed under the skin to position them as close as possible to the tissues of interest to be imaged to maximize the SNR. The lack of connecting cables eliminated the need for transdermal penetrations, reducing the risk of infections. However, some form of biocompatible material is required to insulate the RF coils from the conductive fluids of the animal [16–18]. Here, we are using practical aspects of the inductively coupled coils to manage or avoid the constraints placed on our measurements and imaging of live animals without implanting the coils.

We have designed a series of inductively coupled, transmit-receive coils [19] for X-nucleus and proton MR imaging (MRI) and MR spectroscopy (MRS) in rodent and marmoset. These inductively coupled coils were based on the same design principle [19] but customized for different animal imaging applications, with common aims for the simplicity of the circuit design, ease of use, conforming closely to the anatomy of interest, and achieving a high signal-to-noise ratio (SNR). Each coil set consists of a wireless resonant loop or a volume resonator (saddle or Helmholtz pairs) tuned specifically to the nuclear resonance of interest and inductively coupled to a broadband pick-up loop that is connected to the scanner hardware. In this work, we report the coil designs and demonstrate their utility in hyperpolarized ^{13}C MR spectroscopic imaging (HP13C-MRSI) of pyruvate metabolism in mice, ^{31}P MRS of energy metabolism in rats, and high-resolution ^{1}H anatomical MRI in marmosets.

2. Material and methods

2.1. Hyperpolarized ^{13}C MRSI of pyruvate metabolism in mice

2.1.1. Coil design—For HP13C-MRSI of mouse brain, a wireless resonant loop of 18mm in diameter (Fig. 1A) was made of 16 gauge copper wire with a capacitor tuned to the ^{13}C frequency of 50.38MHz at 4.7T. A variable capacitor (trimmer) was placed in parallel with the fixed capacitor, to allow a small tuning range to compensate for the load. The wireless resonant loop is inductively coupled to a shielded pick-up loop (Fig. 1B) which is connected to the in-system T/R switch, preamplifier, and RF power amplifier. This electrically balanced, untuned, pick-up loop was constructed from semi-rigid coaxial cable (UT-85C-FORM) on a 3D printed mechanical shuttle that was adjusted in position by a screw mechanism to change the overlap between the wireless resonant loop and pick-up coil. An optimal overlap was achieved when matching to the system's 50 ohm impedance. The Bruker system's built in low noise preamplifiers are optimized for a low noise figure for a 50 ohm load. The shield of the semi-rigid coax cable used to eliminate electric field coupling from the coil and/or sample into the pickup loop. The shield is cut at a position opposite the coaxial connection to prevent the shield from electrically shorting out the pickup loop. The

use of a shielded loop is to make the coupling from the resonant loop to the pickup loop, exclusively inductive.

The wireless resonant loop was placed like a crown on the head of a mouse in a prone position (Fig. 1A). Motion of the head was constrained by ear bars and a bite bar. The ear bars also helped to slightly lift the head so that the floating coil was not affected by respiratory motion of the body. This ^{13} C coil was used in conjunction with a Bruker ^{1} H quadrature volume coil of 86mm inner diameter.

2.1.2. Animal experiment—Performance of this coil was first evaluated in SCID mice bearing MGG123 glioblastoma (GBM) tumor [20] in the right hemisphere and we further improved the spatial resolution in normal mice. All animal procedures were performed in accordance with guidelines, regulations, and animal protocols approved by the Institutional Animal Care and Use Committee (IACUC) at Massachusetts General Hospital (MGH). Animals were anesthetized with 2–3% isoflurane mixed with 30% enriched air at 1.5 L/min flow rate. Body temperature was maintained by blowing warm air into the scanner bore. Respiration rate and body temperature were monitored during the imaging session.

A sample of 18 uL [1 $-^{13}$ C]pyruvate or [2 $-^{13}$ C]pyruvate with 30 mM AH111501 was hyperpolarized by dynamic nuclear polarization (DNP) technique in a high-performance polarizer (SpinAligner, Polarize, Frederiksberg, Denmark). Dissolution was performed by using 3.2 mL of dissolution medium (40 mM Trizma PreSet Crystals pH 7.6, 50 mM NaCl, 0.27 mM EDTA, and 50 mM NaOH), yielding 80mM hyperpolarized ^{13} C-pyruvate solution of ~ 7.2 pH for intravenous injection through the tail. Liquid-state polarization was 60% ± 9% for [1 $-^{13}$ C] pyruvate and ~5% less for [2-^{13} C]pyruvate at the time of dissolution. The dissolved HP13C pyruvate solution was transferred from the polarizer to the 4.7T scanner in a hand-held 1.4T magnetic transporter to maintain polarization during the 30s transfer. Polarization at the time of injection was estimated 45% for [1-^{13} C]pyruvate and 35% for [2-^{13} C]pyruvate.

Chemical shift imaging (CSI) started ~10s after the start of HP13C pyruvate injection. Axial CSI was acquired on the GBM model, following a bolus injection of ~200uL of HP [2-^{13} C]pyruvate, with 30 mm × 24 mm field of view, 12 × 10 matrix size, 2.5 mm × 2.4 mm resolution, a single 8 mm slice, 1.08 ms/142.5ms TE/TR, 10° constant flip-angle, centric phase encodings, 100 ppm spectral bandwidth, and 2048 spectral points. Coronal CSI was collected on a normal mouse with a similar CSI protocol but better in-plane resolution of 1.53 mm × 1.53 mm and a thinner slice of 4 mm. The 15s CSI was repeated 6 times following a bolus injection of ~120 uL of HP [1-^{13} C]pyruvate in the normal mouse. Anatomical images were acquired using T_2 RARE. CSI data were analyzed using a custom software in Matlab with 30Hz line-broadening and zero fill once on each of the spectral and two spatial dimensions.

2.2. ^{31} P MRS of energy metabolism in rats

2.2.1. Coil design—To do ^{31} P MRS at 9.4T, we used the same broadband pick-up loop and only had to build another loop resonant at the ^{31} P frequency of 162.26 MHz. This was very simple and economical – a big advantage of the inductively coupled coils. For ^{31} P

MRS of rat brain, a wireless resonant loop of 20 mm in diameter (Fig. 4A) was made of 16 gauge copper wire with a fixed capacitor and a trimmer in parallel for tuning. This ring was taped on the rat head and the pick-up coil was placed on the top, approximately 3 mm above the wireless resonant loop. Matching was performed by adjusting the overlap between the pick-up coil and wireless resonant loop with a built-in screw (Fig. 4A). The Q of the resonant loop was measured with a pair of overlapping but decoupled loops with a vector network analyzer. The decoupling between the loops was below −70dB. When the unloaded resonant loop was placed in proximity to the test loops, the Q was measured to be 296. With a loaded resonant loop, the same double loop method was used and measured a Q of 201.

2.2.2. Animal experiment— ^{31}P MRS was acquired in a Sprague Dawley rat to study energy metabolism. All animal procedures were performed in accordance with guidelines, regulations, and an animal protocol approved by the IACUC of MGH. Animal was anesthetized with 2–3% isoflurane mixed with 30% enriched air at 1.5 L/min flow rate. Body temperature was maintained by blowing warm air into the scanner bore. Respiration rate was monitored during the imaging session.

The inductively coupled coils were tuned and matched on the rat inside a Bruker ^{1}H quadrature volume coil of 86mm inner diameter on a Bruker 9.4T animal scanner (BioSpin, Bruker Corporation, Billerica, USA). High-order shim (map shim) of the rat brain was estimated from B_0 maps acquired over a volume slightly larger than the rat brain. ^{31}P MRS data was collected by a pulse-and-acquire sequence with two sagittal adiabatic saturation bands (hyperbolic secant function), one on each side of the brain, to saturate ^{31}P signal from the muscle surrounding the brain. The free induction decay (FID) data were acquired with a 3s TR, an adiabatic 90° RF pulse (hyperbolic secant), 80.244 ppm spectral bandwidth, 2048 spectral points, 80 averages, and scan time of 4 min. Data were analyzed using a custom software in Matlab with 150 Hz line-broadening. The first 20 points in the FID were removed from processing to reduce ^{31}P signal contribution from the skull, which has a 31P T_2 relaxation time much shorter than that of brain.

2.3. High-resolution ^{1}H MRI of marmoset brain

2.3.1. Coil design—A pair of saddle coils for ^{1}H imaging at 9.4T was built using a combination of 16 gauge copper wire held in a 3D printed former and a pair of curved semicircular copper clad FR4 circuit boards holding the fixed capacitors and a trimmer on each loop (Fig. 5A). One loop was placed below a marmoset's head and the second loop placed over the head yielding a clear space for ear bars. The saddle is inscribed on a cylindrical former with a diameter of 62.5 mm and a length of 50 mm. The semi circular portions of the PCB forming the end of the saddle subtend an angle of 120 degrees. There are two 60 degree gaps between the saddles. The Bruker volume coil was not used in this configuration because the animal, cradle and support structures needed the full 12 cm diameter of the gradient coil. Also, the SNR of the Bruker volume coil is limited because of its much larger diameter.

A pickup loop was held in place by another 3D printed former within the lower loop (Fig. 5B). As this pickup loop is fixed in geometry, variability in the matching was achieved with

a single trimmer capacitor in series with the pickup loop and located 180 degrees away from the coaxial feed point.

Each resonant loop was isolated and tuned to a frequency slightly above the Larmor frequency and when the two elements were moved into the correct positions circumscribing a cylinder, the resonances split into two resonances. The lower frequency is the homogeneous mode where the currents in the two loops circulate in the same direction resulting in a homogeneous RF field and homogeneous sensitivity of the compound coil. The higher frequency resonance is from the differential mode where the two currents circulate in opposite directions yielding a null RF field at the central plane between the two halves of the saddle coil. By tuning the coil in this way, the currents in the lower frequency resonance become equal and the homogeneity of the coils is improved.

As the animal is placed in the coil, the frequency decreases slightly and a trimmer capacitor on one of the saddle elements is adjusted to correct the resonance frequency. Also, at high field, the presence and proximity of an RF shield in the bore raises the frequency slightly. It should be noted our gradient bore diameter is 12 cm and the volume proton coil was not used because of space limitations. The saddle coil was held in place in the animal cradle to minimize variation of the distance to the RF shield of the gradient coil. Impedance matching was achieved by adjusting the small trimmer capacitor in the pickup loop. Some iteration was required as the matching and tuning interact slightly. Two such coils were constructed, one for 9.4T and the other for 3T. In the 3T human scanner, the RF shield lining the gradient coil is sufficiently distant and did not change the resonance frequency of the coil. On the 3T Siemens system, a transmit-receive switch is required to interface with the system and an Advanced Receiver Research (Burlington CT, USA) preamplifier with an optimal noise figure at 50 ohms was used to amplify the signal from the receive side of the T/R switch.

2.3.2. Animal experiment—High resolution proton images were acquired in marmosets at 9.4T and 3T. All animal procedures were performed in accordance with guidelines, regulations, and an animal protocol approved by the IACUC at Massachusetts Institute of Technology. The marmosets were kept under 1 to 2% isoflurane anesthesia under veterinary supervision and placed in ear bars with a palate bar and eye bars to position the head in a standard and reproducible position. A face mask delivers the isoflurane and has been successfully keeping the level of anesthesia constant as measured by heart rate and SPO2. A heated water blanket and thermal insulation was used to maintain body temperature.

At 9.4T, scans were performed using a 3D, isotropic 200 μm resolution, gradient recalled echo (GRE) with TR=20 ms, TE=5.018ms, flip=15°, with RF spoiling. A rapid acquisition with refocused echoes (RARE) sequence was also used to acquire coronal and axial images with an in-plane resolution of 80μm × 80μm with a 1 mm slice thickness.

Very similarly at 3T, a magnetization prepared rapid gradient echo (MPRAGE) sequence was used with TR1=8.4ms, TE=2.58ms, TI=700ms, TR2=2200ms, flip=8°, NEX=3, FOV=70mm, with an isotropic resolution of 360μm. A 3D fast spin echo, T2 sampling perfection with application optimized contrasts using different flip angle evolution (T2-SPACE), was also acquired with matching geometry and TR 3000ms, TE 558 ms, an echo

train length of 160, and a variable refocusing angle schedule with the same spatial resolution and FOV.

3. Results

3.1. Hyperpolarized 13 C MRSI of pyruvate metabolism in mice

Good matching at 50.38MHz was obtained on mouse head as shown in the reflected power curve (Fig. 1C) acquired on the scanner (aka “wobble”), approximately 8% reflected power on resonance. Axial CSI of the GBM model showed large SNR, good image quality and elevated [2-^{13} C]lactate signal on the tumor (Fig. 2), reflecting aerobic glycolysis (the Warburg effect [21]) in GBM. Given the high degree of polarization, we were able to improve the spatial resolution to 9.4μL (or 9.4 mm3) voxel size in the coronal CSI of normal mouse brain (Fig. 3). Large [1-^{13} C]lactate signals lasted in the brain for about a minute. SNR of [1-^{13} C] lactate averaging over 6 frames was 71:1 in the brain and 83:1 in the vessels. SNR of [1-^{13} C]pyruvate was 163:1 in the brain and 283:1 in the vessels.

3.2. ^{31} P MRS of energy metabolism in rats

Good Q and good matching at 162.26 MHz were obtained on rat head as shown in wobble (Fig. 4B), approximately 10% reflected power on resonance. ^{31} P peaks of phosphocreatine (PCr), γ-ATP, α-ATP, and β-ATP were clearly depicted from the ^{31} P spectrum.

3.3. High-resolution 1 H MRI of marmoset brain

SNR maps of the inductively coupled saddle coil at 3T show a homogeneous SNR in both the coronal and sagittal planes (Fig. 5C and 5D, respectively). High quality anatomical images of a marmoset were obtained on a Bruker BioSpec 9.4T scanner using the inductively coupled saddle coils. Fig. 6A shows a sagittal slice of the 3D-GRE image from a 30-min scan. Fig. 6B shows a coronal image of the multi-slice 2D RARE scan acquired with two averages in 17 minutes. Fig. 6C shows a coronal slice of 3D MPRAGE image and Fig. 6D a slice of the 3D T2-SPACE image acquired on a Siemens Prisma-Fit scanner with a saddle coil of an identical form factor tuned for 3T.

4. Discussion

We have shown very simple inductively coupled, transmit-receive coils that can be made easily on the bench with a small budget to achieve good SNR and high image quality in small animals for X-nucleus and proton MR acquisitions. Inductive coupling was used in the dual-tuned ^{1} H/^{13} C quadrature volume coil by GE Healthcare for HP13C-MRSI studies in rodents [13–15]. However, crowning the mouse head with a wireless resonant loop as reported here produced much higher SNR than volume coils because of the close coil proximity to mouse brain and yet was very budget friendly and simple to make. As demonstrated, for MR acquisitions of other X-nuclei, only new resonant loops need to be made and the same pick-up coil can be applied for all. As such, we have multiple resonant loops in our lab, for MR acquisitions of ^{13} C, ^{31} P, ^{2} H, etc.

The HP13C acquisition efficiency can be further improved with more efficient acquisition techniques, such as spectral-spatial selective echo planar imaging (EPI) [10], Spiral-CSI [9], or balanced steady-state free precession (bSSFP) [11,12] type of fast sequences. Better temporal resolution of a few seconds per frame is conceivable with these sequences. The high polarization we were able to obtain from SpinAligner, which was approximately twice of the polarization reported from other d-DNP polarizers, attributed significantly to the high SNR reported here. However, the SNRs from the inductively coupled ^{13}C coil are still remarkable even after scaling the SNRs by a factor of 2 to account for the high polarization we obtained.

We have also demonstrated that inductive coupling also works well for saddle coils, resulting in highly homogeneous RF field, high resolutions, and good SNR. Ultimately, the coil design, the duration of scans and the field strength set upper limits on the SNR of the images. The veterinary staff limited the duration of scan sessions to two hours for these individual marmosets. The vets also determined that the marmosets placed in a sphinx position were the easiest to maintain under isoflurane anesthesia. Therefore, the saddle coil geometry reported here was custom-made for these marmoset studies and to meet addition constraints as follows.

For anatomical imaging, relatively homogeneous B1 field and coil sensitivity profile are desired. A local transmit coil is also desirable to avoid interference with the electrically wired, SPO2 and pulse Ox monitoring equipment. Helmholtz, birdcage, and saddle configurations fulfil these requirements. Receive-only surface coils were also considered but the small size of the elements meant the sensitivity profiles of the coils would be rather small and drop off with distance from the coils. Placing ear bars, the anesthesia mask, and palate bar gave constraints that the birdcage configuration made impractical. For example, the neck of the animal requires extra space in the coil below the head. In earlier experiments, a very short bird cage coil (63mm diameter an 50mm length) was employed leading to a decrease in signal at both the prefrontal and occipital regions of the brain.

The inductively coupled volume coils could be made as a Helmholtz coil but it would be less optimal compared to saddle coils. The spacing between a Helmholtz pair of coils is equal to the radius of the circular elements. A vertically oriented Helmholtz configuration interfered with the shoulders of the animal and a horizontally oriented one with the neck. Larger coils could be built at the cost of SNR.

A saddle coil has a considerable amount of clearance between the two saddle shaped elements yielding room for both the neck and the shoulders of the animals. The saddle coil we designed can be split in half making placement of the animal in the ear bars and face mask, much simpler (Fig. 5B). After placing the animal in the cradle, the top half of the coil can be clipped in place with a 3D printed support to constrain the position and the final resonance frequency. The inductively coupled, splitable saddle coil fulfils the requirements of simplified animal handling and optimal image quality.

One limitation of inductively coupled coils discussed here is that PIN diodes needed to detune the coils are not directly connected to the scanner and would need the addition

of DC path conductors. In a manner similar to the coil matching, mutual inductance can be employed to couple a PIN diode switched detuning loop into the coil structure. A DC bias signal can switch the additional loop on and off to detune the coil during transmission. Alternately, crossed diodes can also be used to passively decouple the coil during transmission. For reasons of simplicity and functionality, we chose to use the described coils as unswitched, transmit-receive coils.

5. Conclusions

Inductively coupled coil design is versatile and practical for X-nucleus and proton MRI/MRS in small animals. High quality images of ^{13}C-pyruvate and its metabolite ^{13}C-lactate were obtained from mouse brain with good spatial resolution and good sensitivity using an inductively coupled coil tailored for HP-^{13}C MRSI of mouse brain. A similar design concept was applied to ^{31}P with a simple construction of a new resonant loop and its utility was demonstrated in ^{31}P MRS of energy metabolism in rat. High resolution proton anatomical images were obtained in marmosets by using a splitable, inductively coupled saddle coil. Ease of use and the ability to make several versions of this coil design to fit different cradle sizes and configurations make the inductively coupled, splitable saddle coil a good choice yielding high SNR and coil homogeneity. Overall, inductive coupling opens up many opportunities for overcoming constraints in the setup of animals while delivering outstanding data quality.

Acknowledgments

We thank the veterinary assistance from Dr. Martina Jackson, Dr. Alexis Mackiewicz, Dr. Ariana Przybylowski, and Dr. Ruoyang Chai. This work was supported by the National Institutes of Health P41EB015896, S10OD021569, S10OD021768, R21GM137227, R01CA227821, UG3H126868, and 5U01EB031641; Seeman Family MGH Research Scholarship in Neuro-Oncology; Stanley Center for Psychiatric Research.

Data availability

Data will be made available on request.

Abbreviations:

MRI	magnetic resonance imaging
MRS	magnetic resonance spectroscopy
MRSI	magnetic resonance spectroscopic imaging
SNR	signal to noise ratio
HP13C	hyperpolarized ^{13}C
DNP	dynamic nuclear polarization
IACUC	institutional animal care and use committee
MGH	Massachusetts general hospital

CSI	chemical shift imaging
FID	free induction decay
GRE	gradient recalled echo
RARE	rapid acquisition with refocused echoes
MPRAGE	magnetization prepared rapid gradient echo
T2-SPACE	T2 sampling perfection with application optimized contrasts using different flip angle evolution
EPI	echo planar imaging
bSSFP	balanced steady-state free precession
PCr	phosphocreatine

References

[1]. Ardenkjær-Larsen JH, Fridlund B, Gram A, Hansson G, Hansson L, Lerche MH, et al. , Increase in signal-to-noise ratio of >10,000 times in liquid-state NMR, Proc. Natl. Acad. Sci. USA 100 (18) (2003) 10158–10163, 10.1073/pnas.1733835100. [PubMed: 12930897]

[2]. Chen Y, Kim H, Bok R, Sukumar S, Mu X, Sheldon RA, et al. , Pyruvate to lactate metabolic changes during neurodevelopment measured dynamically using hyperpolarized 13C imaging in juvenile murine brain, Dev. Neurosci 38 (1) (2016) 34–40, 10.1159/000439271. Epub 2015/11/10. [PubMed: 26550989]

[3]. Choi YS, Kang S, Ko SY, Lee S, Kim JY, Lee H, et al. , Hyperpolarized [1–13C] pyruvate MR spectroscopy detect altered glycolysis in the brain of a cognitively impaired mouse model fed high-fat diet, Mol. Brain 11 (1) (2018) 74, 10.1186/s13041-018-0415-2. Epub 2018/12/20 [PubMed: 30563553]

[4]. Choi YS, Song JE, Lee JE, Kim E, Kim CH, Kim DH, et al. , Hyperpolarized [1–13C]lactate flux increased in the hippocampal region in diabetic mice, Mol. Brain 12 (1) (2019) 88, 10.1186/s13041-019-0505-9. Epub 2019/11/05 [PubMed: 31675964]

[5]. Mikrogeorgiou A, Chen Y, Lee BS, Bok R, Sheldon RA, Barkovich AJ, et al. , A metabolomics study of hypoxia ischemia during mouse brain development using hyperpolarized 13C, Dev. Neurosci 42 (1) (2020) 49–58, 10.1159/000506982. Epub 2020/06/23 [PubMed: 32570236]

[6]. Miloushev VZ, Di Gialleonardo V, Salamanca-Cardona L, Correa F, Granlund KL, Keshari KR, Hyperpolarized (13)C pyruvate mouse brain metabolism with absorptive-mode EPSI at 1T, J. Magn. Reson 275 (2017) 120–126, 10.1016/j.jmr.2016.12.009. Epub 2017/01/07 [PubMed: 28061381]

[7]. Park I, Kim S, Pucciarelli D, Song J, Choi JM, Lee KH, et al. , Differentiating radiation necrosis from brain tumor using hyperpolarized carbon-^{13} MR metabolic imaging, Mol. Imaging Biol 23 (3) (2021) 417–426, 10.1007/s11307-020-01574-w. Epub 2021/01/15 [PubMed: 33442835]

[8]. Peeters TH, Kobus T, Breukels V, Lenting K, Veltien A, Heerschap A, et al. , Imaging hyperpolarized pyruvate and lactate after blood-brain barrier disruption with focused ultrasound, ACS Chem. Neurosci 10 (5) (2019) 2591–2601, 10.1021/acschemneuro.9b00085. Epub 2019/03/16 [PubMed: 30873831]

[9]. Mayer D, Yen YF, Takahashi A, Josan S, Tropp J, Rutt BK, et al. Dynamic and high-resolution metabolic imaging of hyperpolarized [1–13C]-pyruvate in the rat brain using a high-performance gradient insert. Magnetic resonance in medicine: official journal of the Society of Magnetic Resonance in Medicine /Society of magnetic resonance in medicine 2011;65(5):1228–33. Epub 2011/04/19. doi: 10.1002/mrm.22707.

[10]. Miller JJ, Lau AZ, Teh I, Schneider JE, Kinchesh P, Smart S, et al. Robust and high resolution hyperpolarized metabolic imaging of the rat heart at 7 T with 3D spectral-spatial EPI. Magnetic resonance in medicine: official journal of the Society of Magnetic Resonance in Medicine /Society of Magnetic Resonance in Medicine 2016;75(4):1515–24. Epub 2015/05/21. doi: 10.1002/mrm.25730.

[11]. Milshteyn E, von Morze C, Gordon JW, Zhu Z, Larson PEZ, Vigneron DB. High spatiotemporal resolution bSSFP imaging of hyperpolarized [1-(13) C] pyruvate and [1-(13) C]lactate with spectral suppression of alanine and pyruvate-hydrate. Magnetic resonance in medicine: official journal of the Society of Magnetic Resonance in Medicine /Society of Magnetic Resonance in Medicine 2018;80(3):1048–60. Epub 2018/02/17. doi: 10.1002/mrm.27104.

[12]. Milshteyn E, von Morze C, Reed GD, Shang H, Shin PJ, Zhu Z, et al. , Development of high resolution 3D hyperpolarized carbon-13 MR molecular imaging techniques, Magn. Reson. Imaging 38 (2017) 152–162, 10.1016/j.mri.2017.01.003. Epub 2017/01/13 [PubMed: 28077268]

[13]. Derby K, Tropp J, Hawryszko C, Design and evaluation of a novel dual-tuned resonator for spectroscopic imaging, J. Magn. Reson 86 (3) (1990) 645–651, 10.1016/0022-2364(90)90043-9 (1969).

[14]. Albers MJ, Bok R, Chen AP, Cunningham CH, Zierhut ML, Zhang VY, et al. , Hyperpolarized C-13 lactate, pyruvate, and alanine: noninvasive biomarkers for prostate cancer detection and grading, Cancer Res 68 (20) (2008) 8607–8615, 10.1158/0008-5472.can-08-0749. [PubMed: 18922937]

[15]. Spielman DM, Mayer D, Yen YF, Tropp J, Hurd RE, Pfefferbaum A. *In vivo* measurement of ethanol metabolism in the rat liver using magnetic resonance spectroscopy of hyperpolarized [1–13C]pyruvate. Magnetic resonance in medicine: official journal of the Society of Magnetic Resonance in Medicine /Society of Magnetic Resonance in Medicine 2009;62(2):307–13. Epub 2009/06/16. doi: 10.1002/mrm.21998.

[16]. Bilgen M, Magnetic resonance microscopy of spinal cord injury in mouse using a miniaturized implantable RF coil, J. Neurosci. Methods 159 (1) (2007) 93–97, 10.1016/j.jneumeth.2006.06.024. Epub 2006/08/08 [PubMed: 16890294]

[17]. Silver X, Ni WX, Mercer EV, Beck BL, Bossart EL, Inglis B, et al. In vivo 1H magnetic resonance imaging and spectroscopy of the rat spinal cord using an inductively-coupled chronically implanted RF coil. Magnetic resonance in medicine: official journal of the Society of Magnetic Resonance in Medicine/Society of Magnetic Resonance in Medicine 2001;46(6):1216–22. Epub 2001/12/18. doi: 10.1002/mrm.1319.

[18]. Chen YWQ, Zeng H, Takahashi K, Choi S, Qian C, Yu X, ISMRM, Inductively coupled detectors for optogenetic-driven focal and multiregional fMRI signal enhancement, editor, in: Proceedings of the 29th Annual Meeting of the International Society of Magnetic Resonance in Medicine; Virtual 2021, 2023, p. 0133.

[19]. Jl M, Lupu M, Briguet A, NMR Probeheads for Biophysical and Biomedical Experiments: Theoretical Principles & Practical Guidelines, xviii, Imperial College Press, London, 2015, p. 735. Second editionpages p.

[20]. Nigim F, Cavanaugh J, Patel AP, Curry WT, ES-i EM Jr Kasper, et al. , Targeting hypoxia-inducible factor 1α in a new orthotopic model of glioblastoma recapitulating the hypoxic tumor microenvironment, J. Neuropathol. Exp. Neurol 74 (7) (2015) 710–722, 10.1097/nen.0000000000000210. [PubMed: 26083570]

[21]. Warburg O, Über den Stoffwechsel der Carcinomzelle, Naturwissenschaften 12 (50) (1924) 1131–1137, 10.1007/BF01504608.

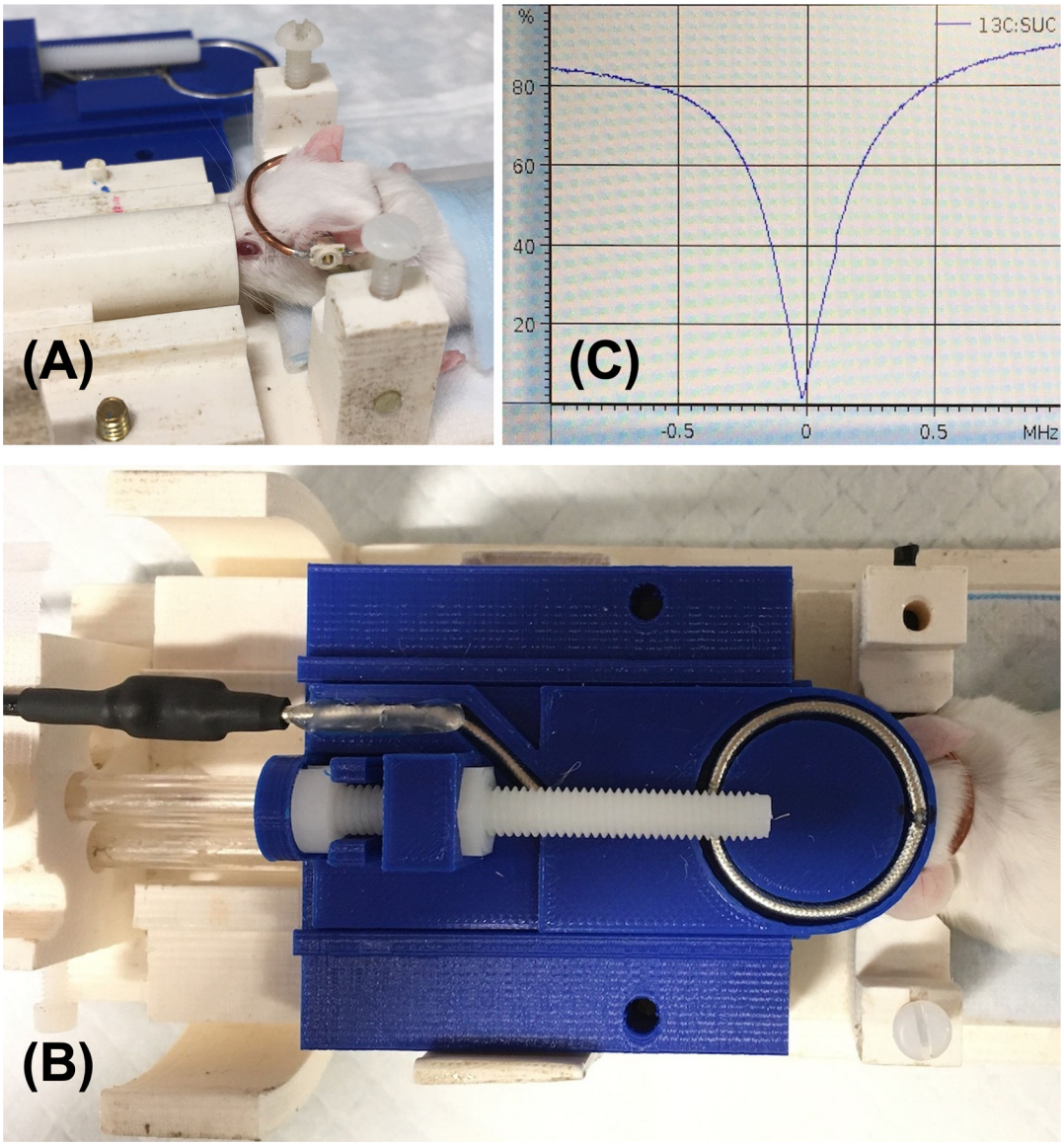

Fig. 1.

Inductively coupled ^{13}C coil for hyperpolarized ^{13}C metabolic imaging of mouse brain. (A) Wireless resonant loop, with a fixed capacitor and a variable capacitor for tuning, placed like a crown over a mouse head. (B) Matching achieved by adjusting the overlap between the shielded pick-up coil and the wireless resonant loop. (C) Excellent matching and tuning demonstrated by reflected power impedance measurement (i.e. wobble) on Bruker 4.7T MRI scanner.

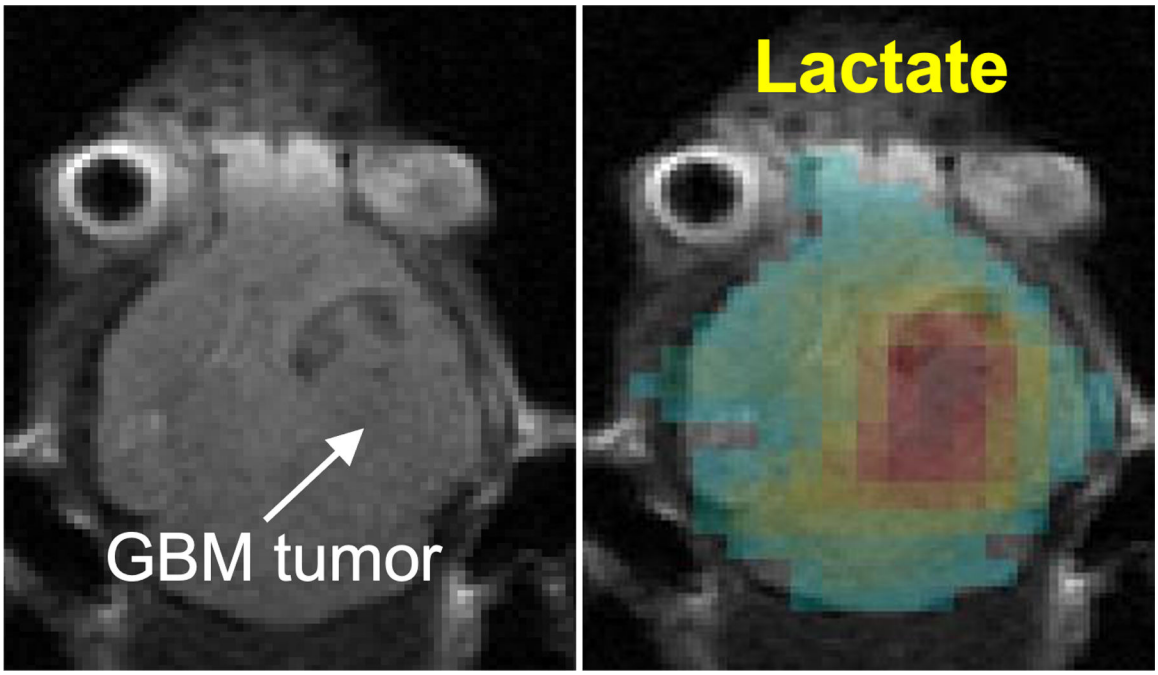

Fig. 2.

[2-^{13} C]lactate image (in colors) of a GBM mouse model (tumor indicated by the arrow) following an injection of hyperpolarized [2-^{13} C]pyruvate. Elevated lactate production in the GBM tumor, as compared to the contralateral side, was observed. Acquired voxel size was 48 μL (48 mm3).

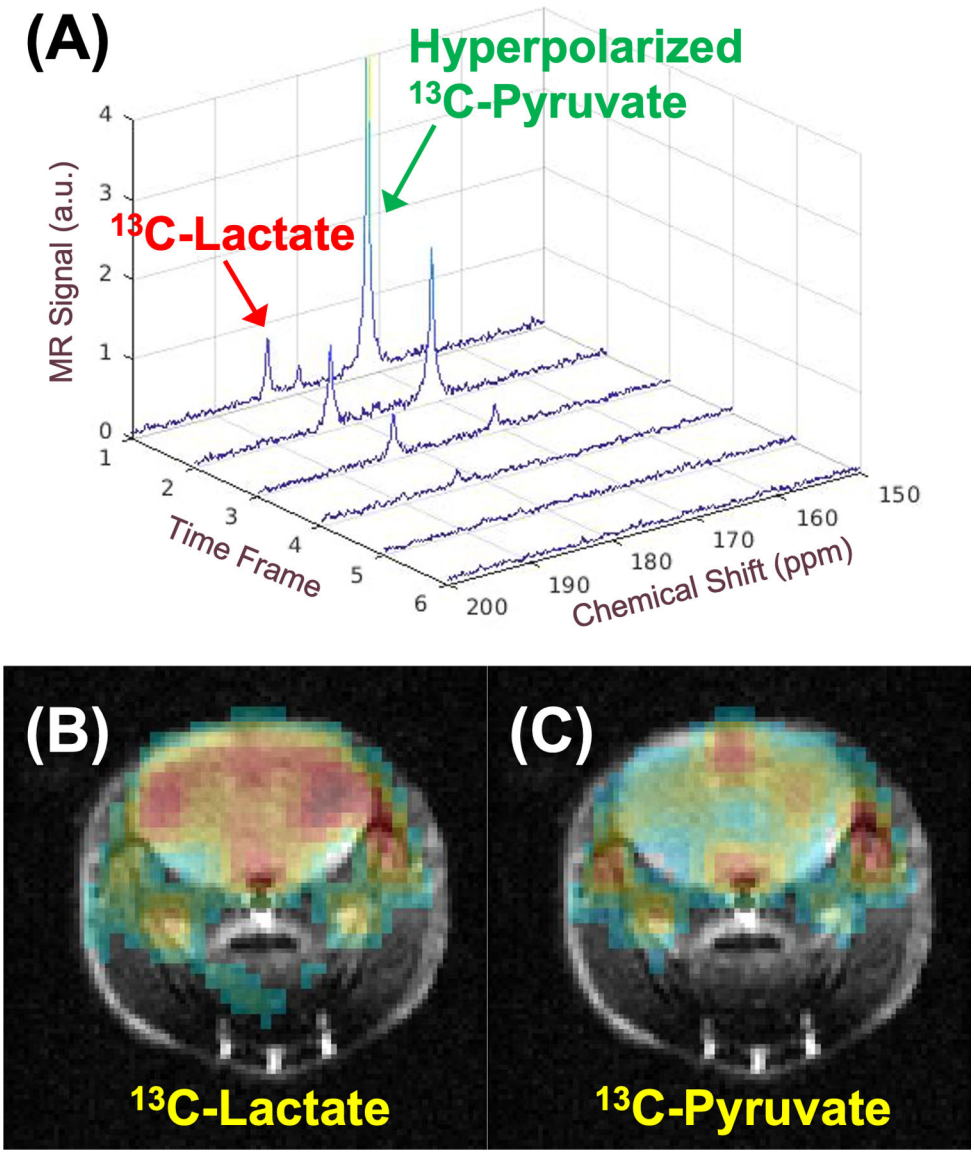

Fig. 3.

Hyperpolarized imaging of pyruvate metabolism in a normal mouse. (A) Stack plots show [1-^{13} C]lactate production from voxels within the brain, following hyperpolarized [1-^{13} C]pyruvate injection and both signals lasted over a minute (15s per time frame). (B) and (C) [1-^{13} C]lactate and [1-^{13} C] pyruvate images (in colors) overlaid on a T2-weighted proton image. Colors are scaled to the maximum signal in each image. Acquired voxel size was 9.4 μL (9.4 mm3).

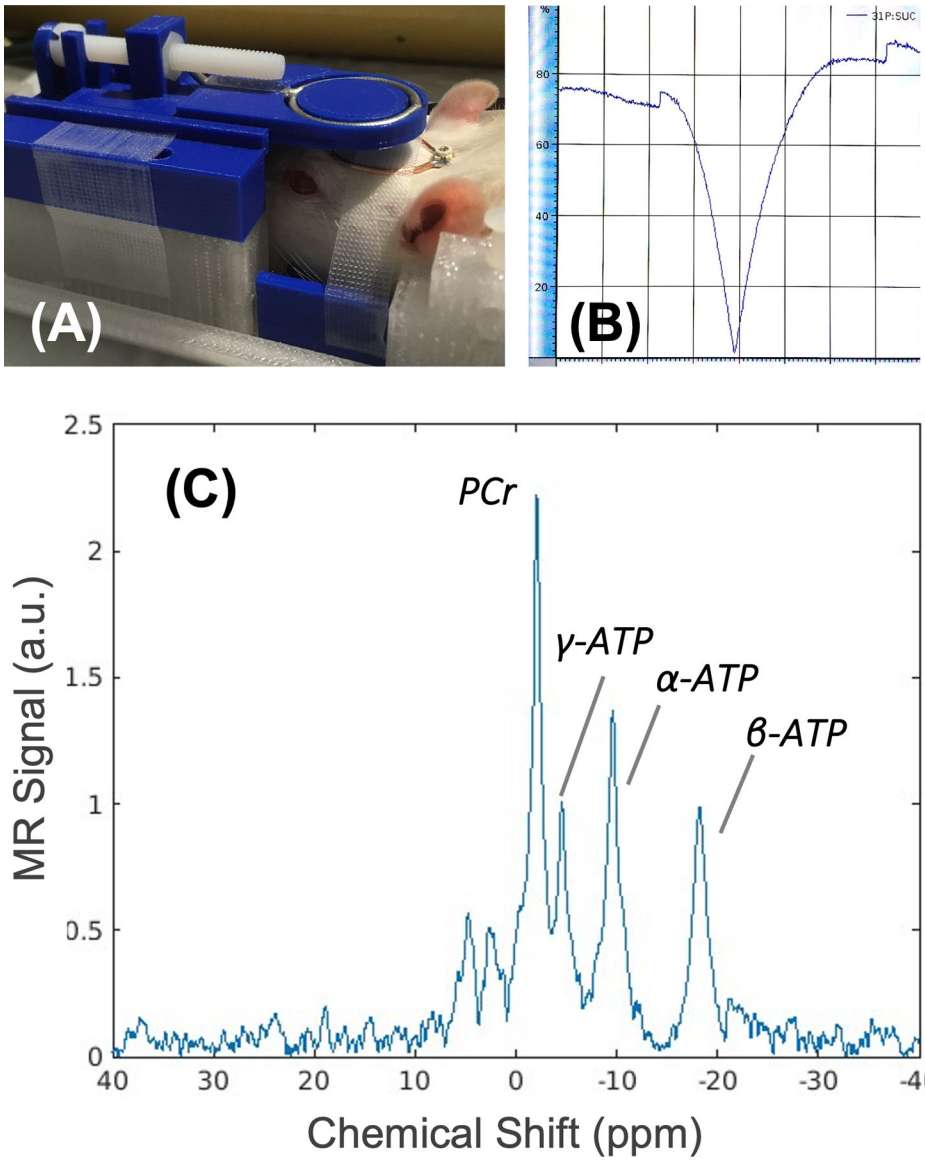

Fig. 4.

31 P MRS of energy metabolism in a healthy rat. (A) A wireless resonant loop tuned to 31 P frequency of 162.26 MHz at 9.4T was taped on the top of rat head and a broadband pick-up coil was placed above the resonant loop. (B) Excellent matching and tuning demonstrated by reflected power impedance measurement (i.e. wobble) on Bruker 9.4T MRI scanner. (C) 31 P spectrum collected in 4 min using a pulse-and-acquire sequence and two sagittal saturation bands, one on each side of the brain, to saturate 31 P signal from the muscle.

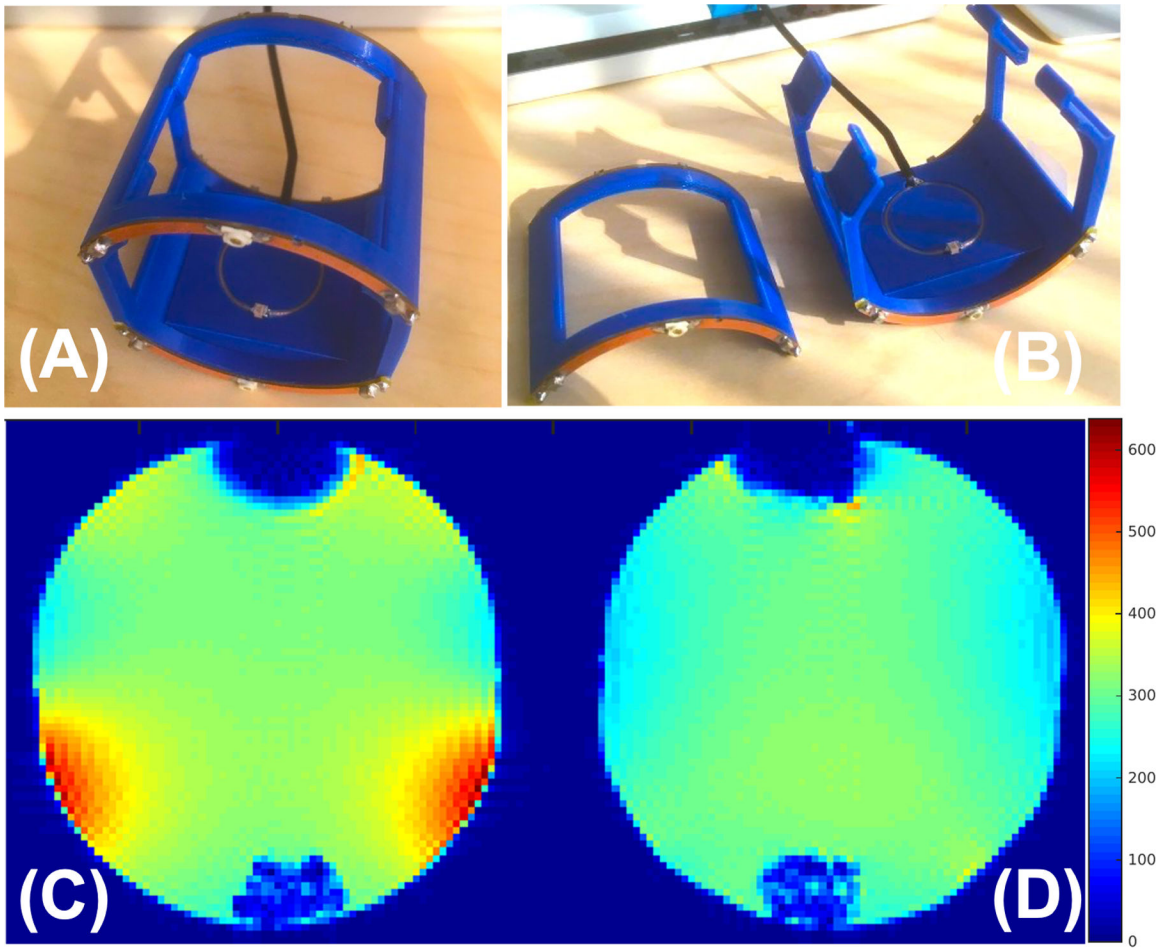

Fig. 5.

Inductively coupled proton saddle coils and SNR maps at 3T. (A) Assembled saddle coils with a pick-up coil embedded in the bottom half of the saddle loop. (B) Splitable design making placement of the animal in the ear bars and face mask much simpler. (C) and (D) SNR maps in coronal and sagittal planes, respectively, of the saddle coil using a 38 mm-diameter sphere containing 1.24 g/L NiSO4 and 2.62 g/L NaCl. The red spots in the coronal SNR map (C) are areas close to the rungs of the bottom saddle loop. The blue signal void at the bottom of the phantom is sediment.

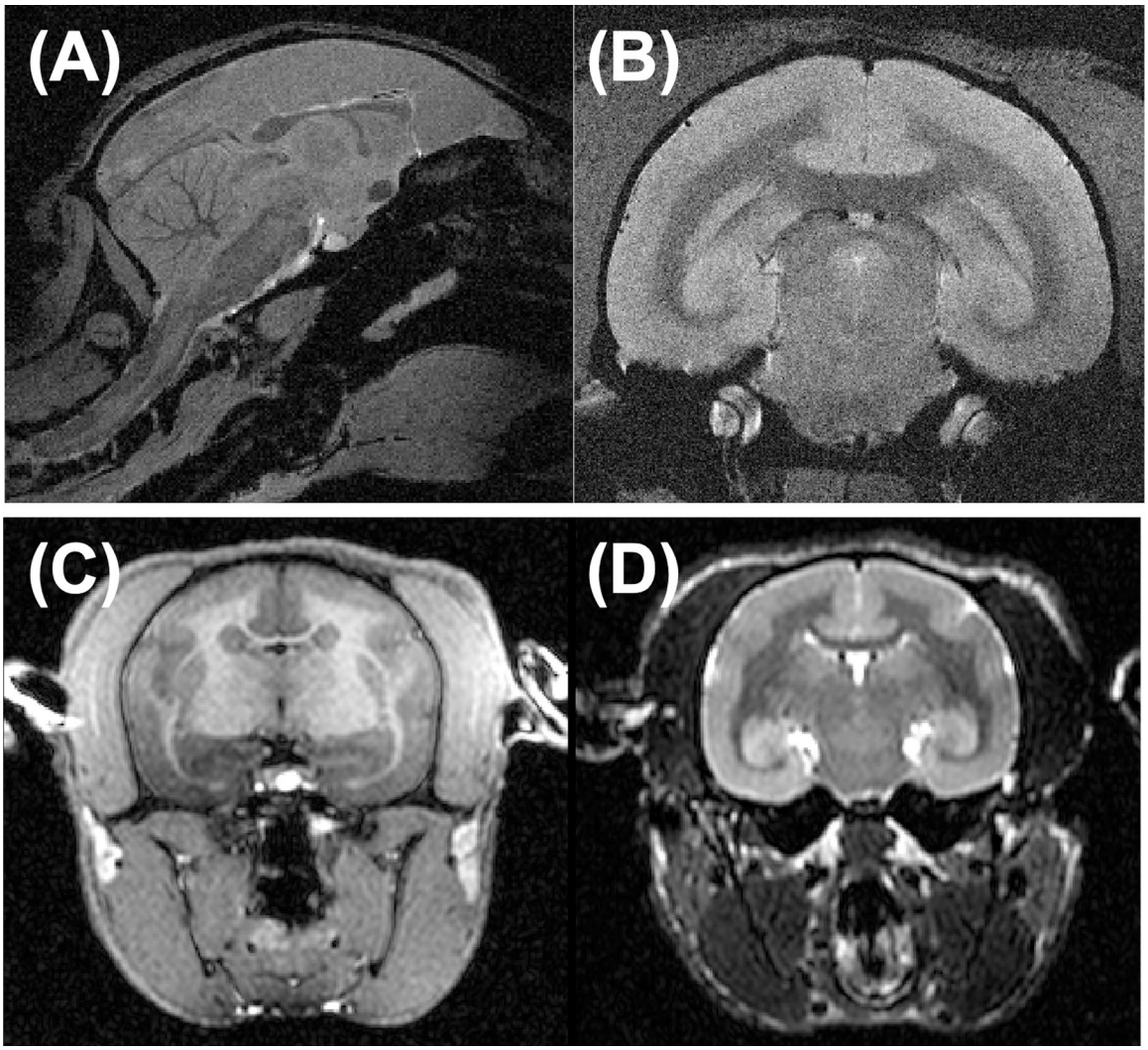

Fig. 6.

High-resolution proton images of marmosets acquired by using inductively coupled saddle coils. (A) and (B) 3D-GRE and RARE images, respectively, of a marmoset at 9.4 T. The spatial resolution of the 3D-GRE image was isotropic 200 μm. The RARE image was acquired with 80 μm × 80 μm × 1 mm resolution. (C) and (D) MPRAGE and T2-SPACE images, respectively, of a marmoset at 3 T with an isotropic resolution of 360 μm.